17th World Conference on Earthquake Engineering, 17WCEE
Sendai, Japan - September 27th to October 2nd, 2021

The difficulty of estimating probabilistic seismic hazard for Lebanon

S.El-Kadri(1), C.Beauval(2), M. Brax(3), Y. Klinger(4), P.-Y. Bard(2)

(1) PhD student, University of Grenoble Alpes, sarah.el-kadri@univ-grenoble-alpes.fr

(2) University of Grenoble Alpes, IRD, University of Savoie Mont Blanc
CNRS, Gustave Eiffel University, ISTerre 38000 Grenoble, France, celine.beauval@univ-grenoble-alpes.fr

(3) National Council for Scientific Research, CNRS-L P.O. Box 16-5432 Achrafyeh 1100-2040, Beirut, Lebanon, brax@cnrs.edu.lb

(4) Université de Paris, Institut de physique du globe de Paris, CNRS, 1, rue Jussieu, Paris, France, klinger@ipgp.fr

Abstract

Keywords: Seismic hazard; Probabilistic forecasting; Lebanon.

Probabilistic seismic hazard assessment (PSHA) consists in determining exceedance probabilities of given ground-motion levels, over future time windows. PSHA relies on source models, that describe the occurrence of future earthquakes, in terms of locations and magnitudes, and on ground-motion models, that predict the ground-motions that these future events may generate. In Lebanon, the observation datasets available both to model earthquake recurrence and to select ground-motion models are scarce. The instrumental catalog (since the sixties) is typical of a low-seismicity region, and is not representative of the large destructive earthquakes that occurred in the past. In the case of the capital city, Beirut, the hazard estimates are controlled by the Mount Lebanon Fault, that is difficult to characterize because located off-shore. In this study, we derive seismic hazard estimates for Lebanon, using various input data (instrumental and historical catalogs, paleoseismology, active faulting), and exploring various source models, to highlight the difficulty of estimating hazard in this region, and to show how much the hazard estimates may vary depending on the input dataset and on the models.

1. Introduction

Lebanon can be classified as a country with high seismic potential since it is located along the Levant fault system (LFS), a ~1200 km long left-lateral strike-slip fault that accommodates the northward motion of the Arabian plate relative to the Sinai-Levantine plate. The slip rate along the LFS has been estimated to be about 5±1 mm/year based on few years of GPS measurements and several hundred thousand of years of geomorphology studies [1]. The present work focuses at establishing a model to forecast future seismic activity in Lebanon and bordering regions. Combining this source model with ground-motion models, a Probabilistic Seismic Hazard Analysis (PSHA) can be led, which aims to evaluate ground-motion occurrence probabilities over future time windows.

Few PSHA studies have been published for this area, and most of them at a regional scale. The most recent seismic hazard maps were delivered by the Earthquake Model of Middle East project that extends from Turkey to Pakistan [2]. Due to the size of the region covered, the epistemic uncertainties on the source model were not fully explored.

This study is part of a long-term project between Lebanon and France, that aims at improving seismic hazard models for Lebanon, through the exploration of the data available, the meaningful models and the associated uncertainties.

2. Smoothed seismicity model

A smoothed seismicity model can be used to forecast off-fault seismicity; this model is based on an earthquake catalog. We use the algorithm developed by Hiemer et al. (2014, SEIFA), that smoothes locations of past earthquakes in space, accounting for completeness in time, and delivers seismic rates maps [3]. The main assumption underlying a smoothed

seismicity model is that future seismicity occurs at, or very close to, locations of past seismicity (e.g. the CSEP worldwide effort, [4]). Note that we use only the catalog part of SEIFA, we do not include faults at this stage.

Strong events have struck Lebanon over the last millennia [5]. However, to build the smoothed seismicity model, we do not consider epicenters of historical events for two reasons: 1) the uncertainty on the epicentral location of these historical events is huge; 2) most of these events occurred on the LFS fault system. Two instrumental catalogs are available, a global catalog, built from global networks, that extends from 1915 to 2015 and includes events down to M_w 4.1 from 1964 on (Brax et al. 2019), and a local catalog, the GRAL, that covers 14 years and includes events down to M_D~2.

2.1 Global catalog (1915-2015)

The global catalog built by Brax et al. (2019) is declustered by applying the Reasenberg (1985) algorithm (parameters in Table 1, Fig. 1a) [6]. The earthquake forecast should be representative of long-term behavior and should not be biased by the presence of aftershock sequences. The Reasenberg algorithm uses spatial and temporal interaction zones to link earthquakes in clusters. The temporal extent of the interaction zone is based on the Omori's law, which describes the temporal decrease of the number of aftershocks after the mainshock. In space, the algorithm assumes a circular rupture radius for each event and searches in this area for foreshocks and aftershocks.

Applying SEIFA algorithm, a spatial density map is obtained by smoothing every earthquake epicenter. A spatial kernel is applied; the level of smoothing depends on the density of earthquakes. The smoothed seismic rate map obtained displays annual exceedance rates for earthquakes with M_w larger or equal to 4.5 (Fig. 1b). To each cell is associated a b-value estimated at the regional scale (Fig. 1c). We observe that the largest seismic rates are related to the 1956 (M_w 5.6) and 2008 (M_w 5.1) earthquake locations.

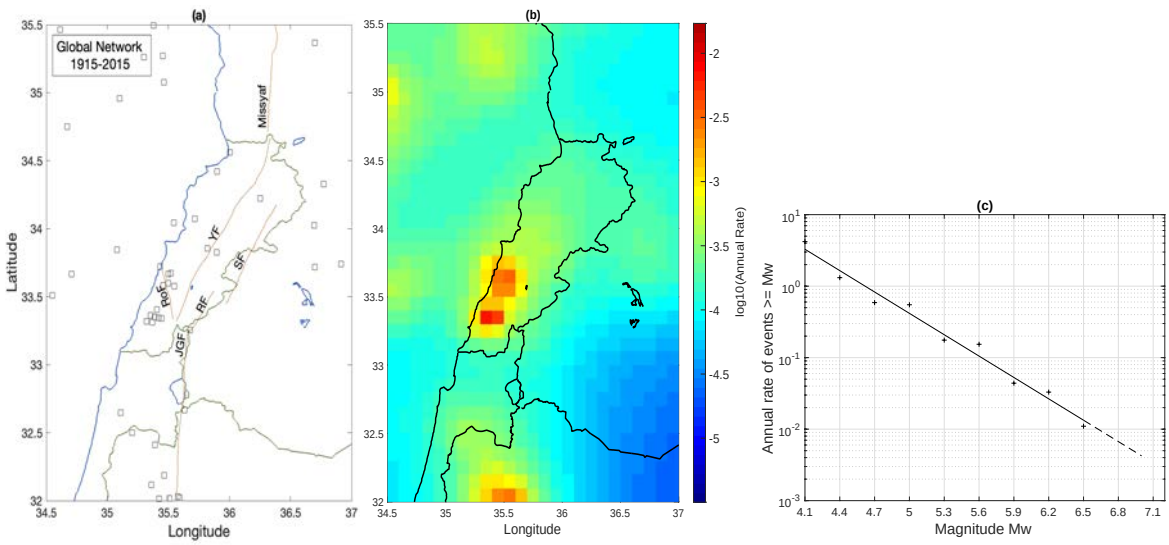

Fig. 1 – (a) Global earthquake catalog (1915-2015, Brax et al. 2019) after declustering, M_w 4.1+, (b) smoothed seismic rates M_w 4.5+, (c) frequency-magnitude distribution based on the declustered catalog.

2.2 GRAL local catalog (2006-2019)

The GRAL catalog covers only 14 years, but it goes down to ~M_D 2.0 (Fig. 2). This low-magnitude seismicity delineates patterns in and around Lebanon that may be used to predict future low-to-moderate earthquakes, assuming that these patterns are somehow stable in time. Again, we apply the Reasenberg (1985) algorithm. We decided to use the parameters indicated in Table 1, that delivers 4165 mainshocks out of 7342 earthquakes (fig. 2a). Based on this catalog, we establish a frequency-magnitude distribution (Fig. 2b, crosses). The result shows two slopes, with a b-value equal to 1.2 over the linear magnitude range 3.3-5, and a much higher slope for lower magnitudes. Reasenberg (1985) was not made for such low-magnitude seismicity; nonetheless it identifies many swarms within Lebanon (Fig.3). We perform a sensitivity study to understand how the declustering parameter choices influence the results. Varying the declustering

parameters within meaningful ranges, we get different amounts of clustered events, but the resulting frequency-magnitude distributions still have the same behavior with two slopes.

Another declustering algorithm is tested on the GRAL catalog, using the J. K. Gardner and L.Knopoff, 1974 [7]. This method is known as a window method and is one of the simplest forms of aftershock identification. It is known to identify more clustered events than the Reasenberg algorithm [8]. This method ignores secondary and higher order aftershocks (i.e., aftershocks of aftershocks). Here we apply this algorithm with the time and spatial windows defined in Grünthal (1985), calibrated on aftershock sequences in Europe. The final mainshock catalog contain 637 events (Fig. 4a). Still, the frequency-magnitude distribution obtained displays two slopes, with a b-value of 1.1 for magnitudes larger or equal to 3.3 (Fig. 4b).
The observation of two slopes in the frequency-magnitude distribution is unusual; the model can only be used in the upper magnitude range where the slope obtained is within the range commonly observed in nature (around 1.0). The two slopes may have different causes: the way the duration magnitudes are determined; the presence of non-tectonic earthquakes; or a true behavior revealing some physical processes in the area.

Table 1 - Parameters of the Reasenberg algorithm used to decluster the instrumental catalogs.

Parameters	Global Catalog	GRAL Catalog
rfact	20	20
x_{meff}	4.1	2
x_k	0.2	0.2
P	0.99	0.99
Tmin (days)	10	10
Tmax (days)	30	30
Uncertainty on the locations	Taken into consideration	Not considered

Given the presence of many swarms in the catalog, we perform some tests to detect earthquakes that would be related to human activities (such as quarries). A sliding spatial window is applied, the distribution of the number of events versus the hour of the day is analyzed within circles of radius 15 km. In some areas, the distribution displays an expected shape, no difference appears between the day and the night activity (Fig. 5a). However, in many areas within Lebanon, an unexpected distribution is obtained, with many more events during the day than during the night (Fig. 5b). This difference in the number of events recorded clearly indicates shocks related to human activities. These shocks are only partially discarded during the declustering process.

A detailed analysis of signals would be required to properly extract shocks related to human activities from the catalog. For now, we test the establishment of the smoothed seismicity model based on night periods only. Applying the Reasenberg declustering on a catalog where working hours have been excluded, we obtain the frequency-magnitude displayed on Fig. 2b (circles), with a linear slope equal to 1.3 over the magnitude range 3.6-4.2. Applying the Gardner and Knopoff declustering on the same catalog, we obtain the frequency-magnitude distribution displayed on Fig. 4b, with a linear slope equal to 1.4 over the magnitude range 2.8-4.2.

2.3 Two smoothed seismicity models selected for hazard calculation

Depending on which catalog is used and which declustering is applied, the pattern of the smoothed seismicity model may change considerably. We decide not to use the model that relies on the Mw4.1+ events in the global catalog, as the forecast would be too much related to the two earthquake sequences that occurred in 1956 and 2008. Instead, we prefer to take advantage of the low-seismicity GRAL catalog, assuming that these zones of high earthquake densities may be the focus of future events. For now, the maximum magnitude that we will be considering for this off-fault seismicity is arbitrarily fixed to Mw 6.0. To account for the uncertainty related to the choice of the declustering algorithm, the choice of the magnitude range to determine the b-value, and the decision on keeping only events occurring during the night, we select two alternative models for the hazard calculations, based on:

- The GRAL catalog declustered with Reasenberg (1985), including all earthquakes with magnitudes M_D3.3+, and a b-value of 1.2. (Smoothed Model 1; Fig. 6, 1st row)
- The GRAL catalog declustered with Gardner and Knopoff (1974), including night earthquakes with magnitudes M_D2.8+, and a b-value of 1.4. (Smoothed Model 2; Fig. 6, 2nd row))

The magnitudes in the GRAL catalog are duration magnitudes M_D. Given the difficulty to establish a conversion equation from M_D to M_w [5], for now we assume that M_D magnitudes are surrogates for M_w magnitudes. Fig. 6 displays the two alternative smoothed seismicity models obtained that will be used in the hazard calculation.

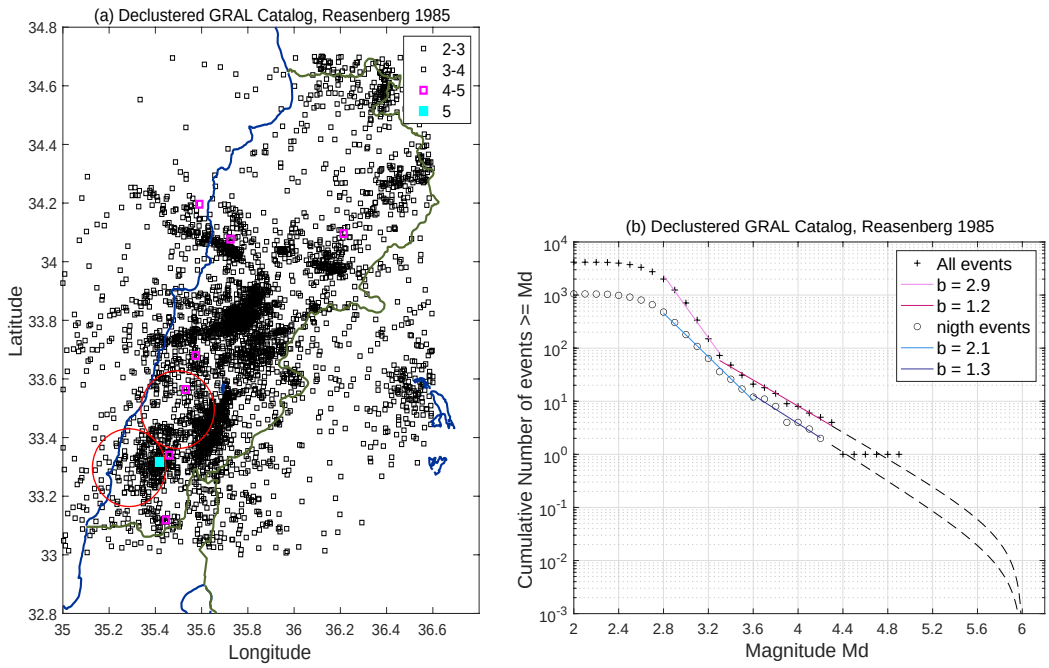

Fig. 2 – (a) Declustered GRAL earthquake catalog applying Reasenberg (1985) algorithm, (b) corresponding frequency-magnitude distributions assuming a maximum magnitude of 6. Circles in fig.2a corresponds to the human activity analysis explained in fig.5

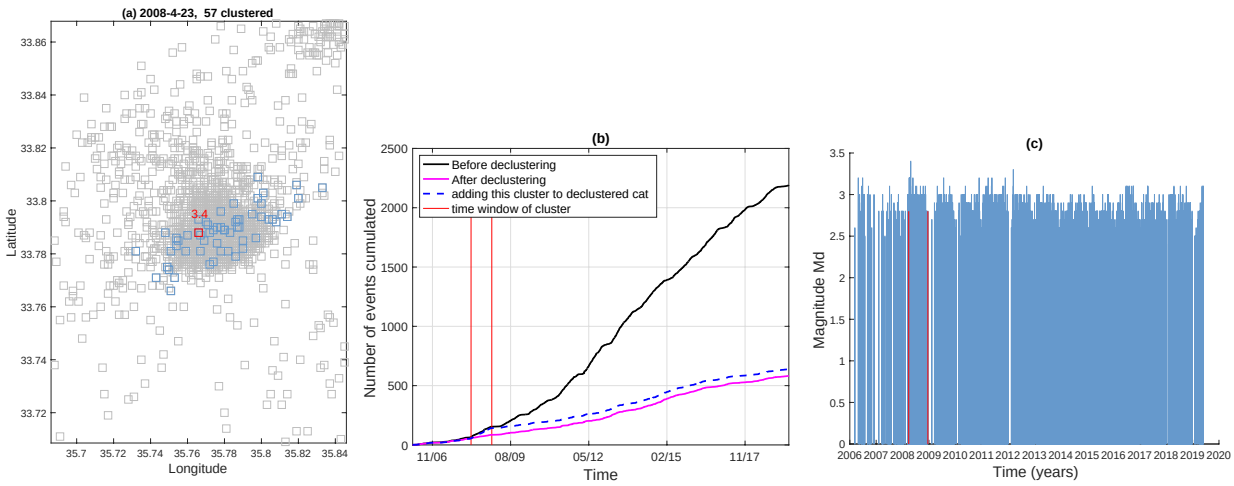

Fig. 3 – Illustration for Reasenberg declustering, example in a region with many swarms. (a) the cluster identified in blue, (b) the cumulative number of events versus time, within the spatial window in (a); black: original catalog; magenta: declustered catalog; blue: declustered catalog with the cluster added; (c) magnitude versus time, original catalog within spatial window in (a); cluster identified by red bars.

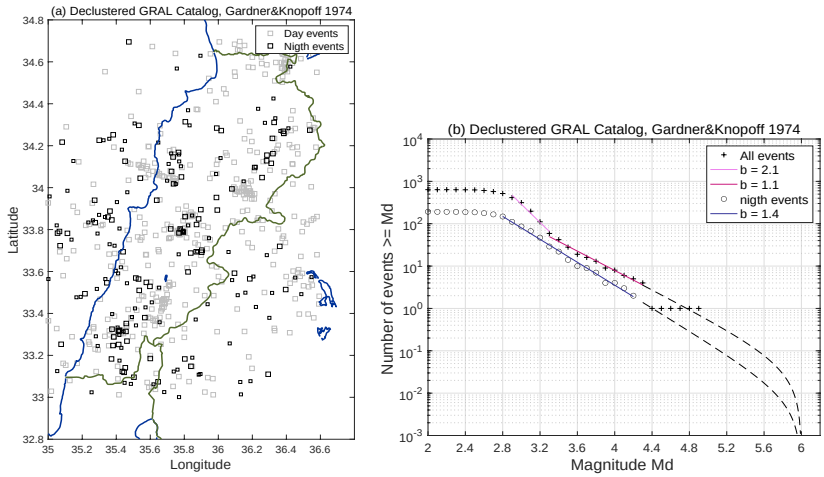

Fig. 4- (a) Declustered GRAL catalog applying Gardner&Knopoff (1974); (b) corresponding frequency-magnitude distributions.

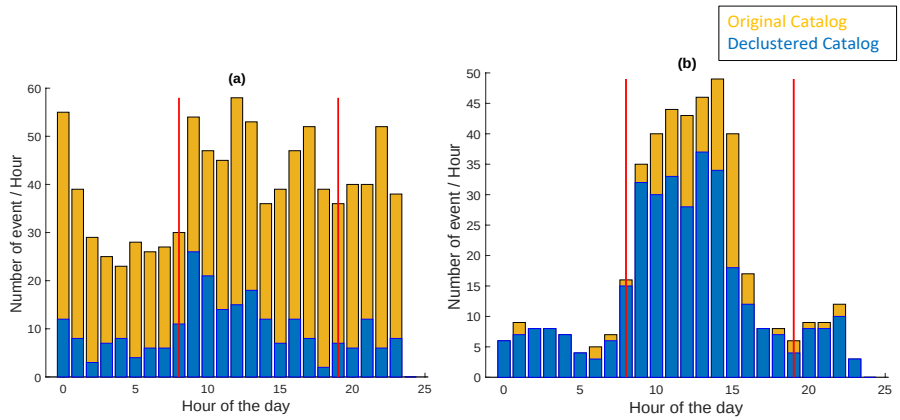

Fig. 5- Distribution of earthquakes according to the time of the day, working hours delimited by red bars; (a) example of expected distribution for tectonic events, within the circle in fig.2a (center lat:33.3, lon:35.3), (b) example of unexpected distribution, within the circle centered on lat:33.5, lon:35.5.

3. Fault Model

A fault model is combined with the smoothed seismicity model. The smoothed seismicity model forecasts earthquakes up to a maximum magnitude of 6.0 and we assume that larger events are generated on the faults. For now, we make the hypothesis that earthquake occurrences on faults follow a Gutenberg–Richter exponential distribution, bounded by maximum magnitudes inferred from the dimensions of the faults. The rate of earthquakes is then inferred from the geological slip rate estimates. For the present calculations, we use a value of M_w6.0 for the maximum magnitude in the background and for the minimum magnitude on the faults.

3.1 Defining the Set of Active Faults

In the present work, we will consider only major faults affecting the Lebanese region, we don't take into account the secondary fault segments that are not well-characterized (many of them NE-SW oriented, no estimate for the slip rate). The Levant Fault System (LFS) can be divided into two North-South trending sections connected by an approximately 170 km long bend, the Lebanese restraining bend [9]. The LFS splays within the bend into the main Yammouneh fault and three secondary branches: Rachaya, Sergaya, and Roum faults. The longest and most active fault is the Yammouneh fault, which has a left-lateral strike-slip mechanism (Fig. 7). It extends from the Southwest to the Northeast over approximately 170 km, connecting the northern to southern section of the LFS. Daëron et al. (2007) estimated its slip rate between 3.8 and 6.4 mm/yr, based on cosmogenic dating of offset alluvial fans [10].

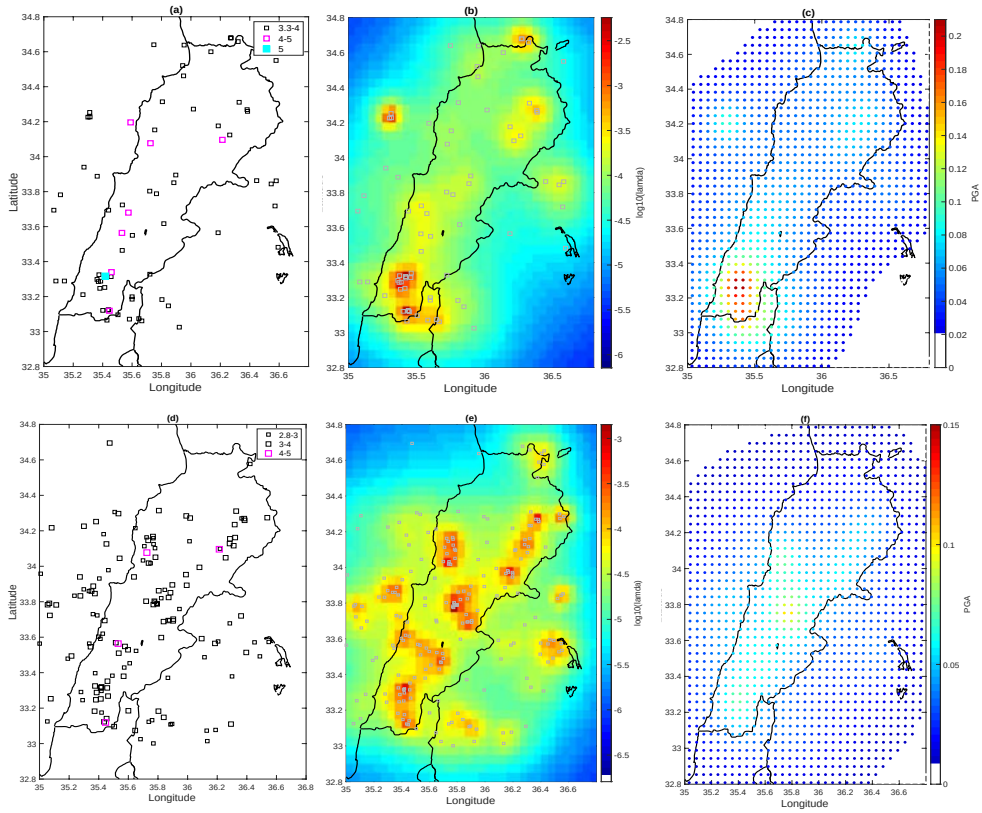

Fig. 6 - (a) Declustered GRAL catalog, using Reasenberg (1985), events with M_D 3.3+ used for the smoothed seismicity model, (b) corresponding annual exceedance rate forecasts for magnitude M_D>=4.5, (c) corresponding seismic hazard map, (d, e, f) same graphics, using this time the catalog declustered with Gardner&Knopoff (1974), keeping night-time events M_D 2.8+ used in the smoothed seismicity model

The Roum Fault bounds to the south Mount Lebanon range, it extends over ~40 km. Nemer and Megraoui (2006) estimated a slip rate from 0.86 to 1.05 mm/yr based on left lateral stream offsets that may have been accumulated through coseismic displacements during the last 10,000 years [11]. The Serghaya (~90 km) and Rachaya (~40km) extend along the Anti-Lebanon range and show left-lateral strike-slip movement. Gomez et al. (2003) assigned them a slip rate of 1.4 ± 0.2 mm/yr during the Holocene, based on a paleoseismological study along the Zabadani valley [9]. The Mount Lebanon thrust is located off-shore Lebanon. It accommodates most of the shortening motion associated to the restraining bend of the LFS. Elias et al. (2007) estimated a slip rate between 1 and 2 mm/yr [12].

The Jordan Gorge fault belongs to the section of the LFS to the south of the restraining bend. Wechsler et al. (2018) estimated a slip rate for the last four millennia of $4.1^{+0.4}/_{-1}$ mm/yr [13]. The Missyaf segment belongs to the section of the LFS north of the restraining bend. It extends approximately over 70 km. Sbeinati et al. (2010) determined a slip rate ranging from 4.9 to 6.4 mm/yr based on paleo-archeoseismic study over the past 3,500 years [14].

3.2 Characterization of faults

The seven crustal faults are included in our source model (Fig. 7). Table 2 summarizes the main parameters required for including the faults in the hazard calculation. We consider that all the deformation will be released in earthquakes; no evidence of creep has been demonstrated for the present time. Strike-slip faults are assumed to be vertical (dip 0°). A dip of 45° is assumed for the Mount Lebanon Fault [12]. All faults extend down to 15km depth. Based on the literature, we associate some historically significant earthquakes to the different faults. Magnitude estimates for these events are retrieved from the Brax et al. (2019) earthquake catalog. The maximum magnitude that may break a fault is determined considering both a scaling relationship (Leonard, 2010) and the magnitude of the historical event associated to the fault [15].

If all of the accumulated deformation is released in earthquakes, the annual seismic moment rate on the fault can be estimated as $\dot{M}_0 = \mu A \dot{S}$, in which $\dot{S}$ is the slip rate per year, μ is the shear modulus (taken as 3.6 x 10^{10} N/m^2), and A is the rupture area. We need to choose a model to distribute the seismic moment rate that will be released on the fault through earthquakes of various magnitudes. The Anderson & Luco (1983) exponential function N2 is selected, constrained by the slip rate, a b-value, and the maximum magnitude on the fault [16]. The a-value for each segment is calculated as follows:

$$10^a = \dot{M}_0 \frac{c-b}{b} 10^{-d+(b-c)M_{max}} \qquad (1)$$

where c and d are the coefficient to estimate the seismic moment from the moment magnitude. The b-value applied to the fault is around 1.0. The b-values calculated from the GRAL catalog are higher (1.2-1.4), but they are not representative of a long-term behavior. A b-value around 1.0 was found from the global Brax et al. (2019) catalog (1915-2015), and this is the most common value found for b in nature. As there is considerable uncertainty on this parameter, a b-value arbitrarily set to 0.85 will also be tested. The parameters used to characterize faults bear considerable uncertainties. Some of these uncertainties will be accounted for in the present hazard calculations. We will quantify the impact on hazard making different assumption of the slip rate value.

4. Ground-Motion Model

To assess probabilistic seismic hazard, the source model must be combined with a ground-motion prediction model. Based on the EMME project, where models have been tested against data in the Middle East region [2], we use the following equations:

- Akkar & Çağnan (2010), relying mostly on Turkish data [17].
- Akkar et al. (2014), Model established from a European and Middle East database (RESORCE) [18]
- Chiou, Brian S. J.Youngs (2014), Next Generation Attenuation project, based on Western US data for small to moderate magnitudes, and global data for larger magnitudes [19].

The aim is to sample the epistemic uncertainty on the prediction of ground motions in Lebanon. The 3 models are equally weighted in the logic tree.

5. Hazard calculations

A logic tree is set up to account for some of the uncertainties that characterize the models built and propagates them up to the hazard estimates (Fig. 8). Two alternative smoothed models are included (Section 2). As for faults, we tested different values of the slip rate (minimum and maximum bounds, mean estimate), as well as different b-values for modelling the Gutenberg-Richter recurrence. We also consider minimum and maximum bounds for M_{max} (Table 2). We aim at exploring different branches of the logic tree to understand which parameter(s) control the hazard in Lebanon. The minimum magnitude used in the hazard calculations is M_W4.5.

5.1 Impact of the choice of the smoothed seismicity model

At first, we evaluate the impact of the smoothed seismicity model on the hazard levels. Fig. 9a and 9b display the mean seismic hazard maps obtained for the PGA at 475 years return period. Each hazard map is obtained by keeping the smoothed seismicity model fixed but exploring the rest of the source model logic tree, and the ground-motion model logic tree. Both resulting maps are very similar. For most sites located in-between faults, the fault contributes more to the hazard than off-fault seismicity. In Beirut (Fig. 9c), the choice of the smoothed seismicity model has no influence on the uniform hazard spectrum (UHS) at 475 yrs. Nonetheless, for a few sites, away from the faults, the impact can be non-negligible (example site on Fig. 9c).

5.2 Impact of the hypothesis on the slip rate

The mean seismic hazard maps in Fig. 10 have been calculated making different assumptions on the amount of the deformation considered. If we use the upper bound of the slip rate, acceleration values at 475 years return period reach ~0.6g along the Yammouneh fault. If we use the minimum bound instead, i.e. a smaller amount of $\dot{M}_0$ is available to generate earthquakes, hazard values along the Yammouneh fault are much lower, around ~0.5g. The slip rate assumed on the fault has a major impact on the hazard levels.

5.3 Focus on Beirut

5.3.1 The hazard in Beirut is controlled by the Mount Lebanon Fault

We focus on Beirut, the capital city located on the hanging wall of the Mount Lebanon thrust, at around ~20 km from the Yammouneh fault. In order to understand which fault contributes the most to the hazard in Beirut, we calculate hazard accounting for the full fault model, then we take into account only the Mount Lebanon Fault. Results for the PGA show that for exceedance probabilities lower or equal to 10% (over 50 yrs, i.e. return periods larger or equal to 475yrs), the hazard is fully controlled by the Mount Lebanon Fault (Fig. 11). The other faults have a negligible contribution.

5.3.2 Impact of the b-value

Here we consider only one branch of the logic tree (mean slip and M_{max} 7.7 for the Mount Lebanon thrust). Fig. 12 shows the impact of different b-values on the frequency-magnitude distribution of the fault. Varying the b-value from 1 to 0.85, the rate of magnitudes below ~M_w6.6 decreases, whereas the rate above this magnitude increases. The corresponding UHS in Beirut, at 475 years return period, are displayed in Fig. 12b. A decrease in the b-value from 1 to 0.85 leads to a decrease in the hazard levels, at all spectral periods. At 475 yrs, the earthquakes with magnitudes lower than 6.6 contribute more to the hazard than larger magnitude events.

5.3.3 Impact of M_{max}

If now we keep fixed the b-value and the seismic moment rate (with assumptions of mean slip rate and b=1), an increase of M_{max} from 7.1 to 7.7 on Mount Lebanon fault leads to a decrease of annual rates for all magnitudes below ~6.9. As a consequence, an increase of M_{max} leads to lower hazard levels, as shown in Fig. 13.

5.3 Which parameters control the hazard in Beirut?

The variability on the hazard levels obtained by exploring the full logic tree is displayed in Fig. 14 (24 branches, in grey). Then we group the acceleration estimates to understand the impact of choices made while building the source model. Mean acceleration values are reported as well as the percentiles 16th and 84th. In order to quantify the impact of the slip rate estimates, the 24 accelerations are split into three groups: accelerations obtained assuming respectively minimum (1 mm/yr), mean (1.5 mm/yr) and maximum slip rate (2 mm/yr). In order to quantify the impact of the assumptions on the b-value and of M_{max}, the accelerations are split respectively into two groups. This plot enables to visually identify which parameter is responsible for the largest uncertainty on hazard levels: the uncertainty on the slip rate and on the maximum magnitude are the parameter that impacts the most the hazard. The uncertainty on the b-value and on the off-fault seismicity model have a negligible impact. Very similar conclusions can be derived at 0.2s and 1s spectral period (Fig. 14).

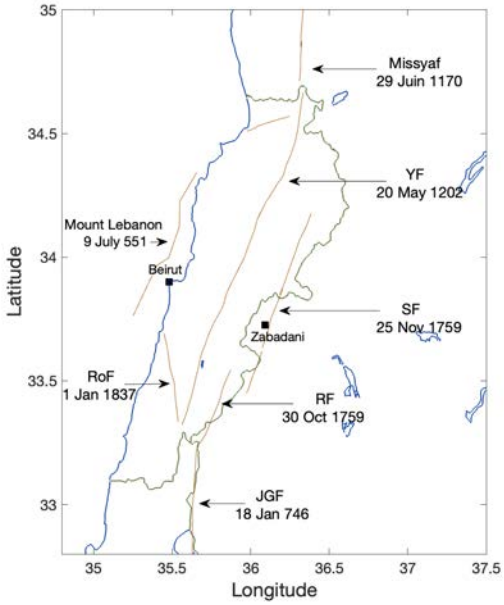

Fig. 7 - Major crustal faults included in the source model, with the associated historical event.

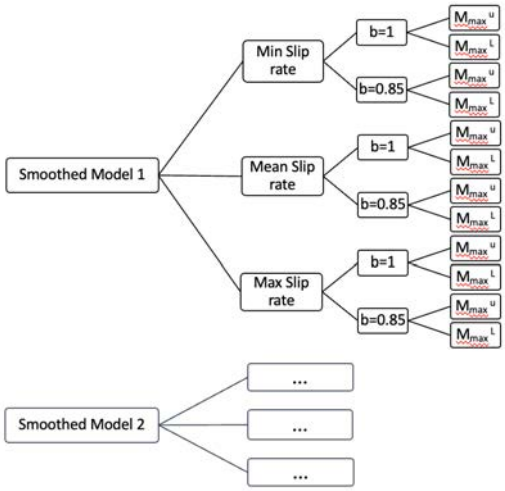

Fig. 8- Source model logic Tree

5. Conclusions

We have presented the first steps in a long-term project aimed at estimating PSHA in Lebanon. To build the earthquake forecast, a smoothed-seismicity model is combined with a fault model. Uncertainties on the parameters characterizing the input source model are propagated up to the final hazard estimates. Within the assumptions made, i.e. that earthquake frequencies on faults follow a Gutenberg-Richter exponential model and can be constrained by geological slip rate estimates, the off-fault seismicity model has a rather negligible contribution on hazard, for return periods larger or equal to 475 yrs. Moreover, our exploration of uncertainties demonstrates that for Beirut city, at least two parameters control the hazard levels: the estimate of slip rate on the fault, and the estimation on the maximum earthquake that could break the Mount Lebanon fault. We acknowledge that some decisions taken in the building of the source model are quite arbitrary: e.g. M_{max} for earthquakes in the background, range of magnitudes considered on the faults, assumption of a Gutenberg-Richter model for faults. These decisions impact strongly the hazard levels. More work is required to have a comprehensive understanding of the hazard levels and controlling parameters in Lebanon. Other models should be tested. A more complex source model logic tree should be built, potentially leading to a larger variability on hazard levels than the one obtained in the present study.

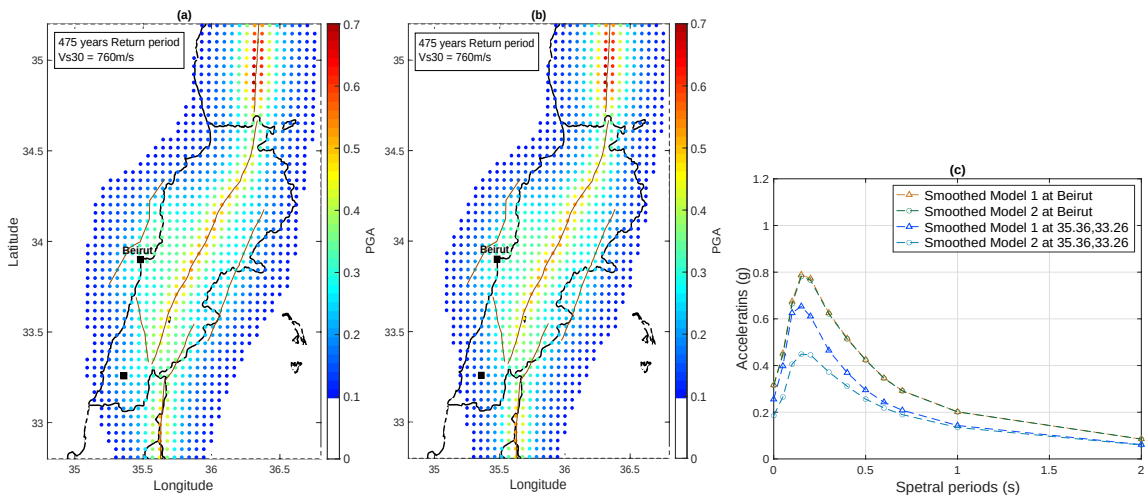

Fig. 9 - Mean seismic hazard maps, PGA, 475 years return period, for a generic rock site with V_{s30}=760 m/s, exploring the full logic tree but keeping the smoothed seismicity branch fixed. (a) Smoothed model 1; (b) Smoothed model 2; (c) corresponding UHS at 475 years, in Beirut and at the site coordinate (35.4,33.25), black squares on the maps.

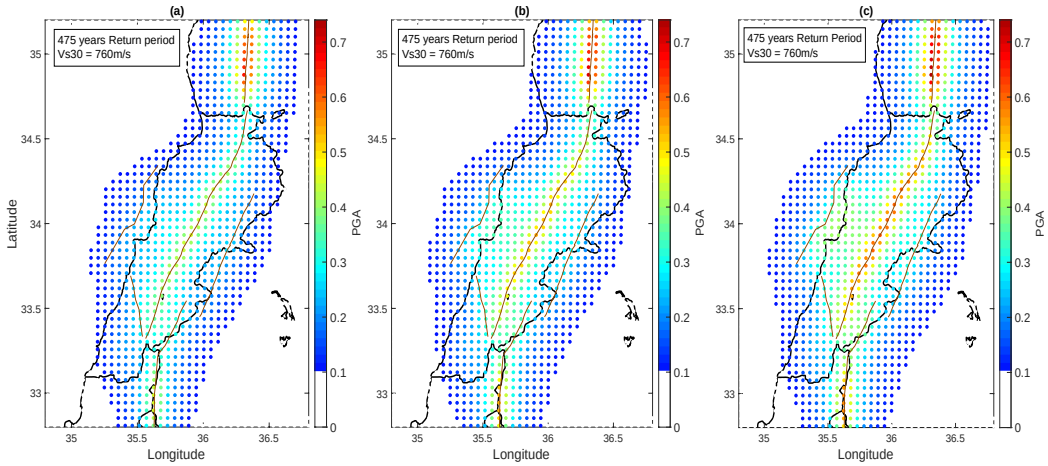

Fig. 10 – Mean hazard maps, PGA at 475 years return period, for a generic rock site with Vs30=760 m/s, corresponding to (a) minimum slip rate, (b) mean slip rate, (c) maximum slip rate, assumed for all faults in the model (see fault parameters in Table 2).

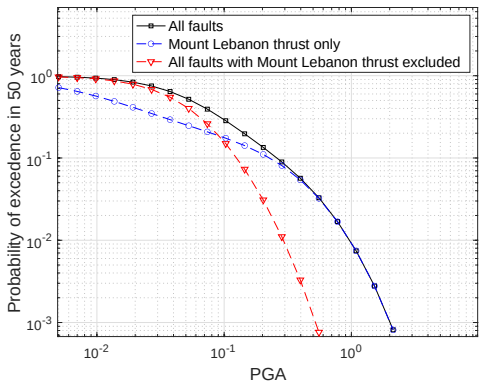

Fig. 11- Mean hazard curve for the PGA at Beirut, considering the fault model (7 faults, black), then taking into account only Mount Lebanon thrust fault (blue). The hazard curve in red is obtained considering the 6 other faults in the model. Hazard calculations led with mean slip rates and a b-value equal to 1.

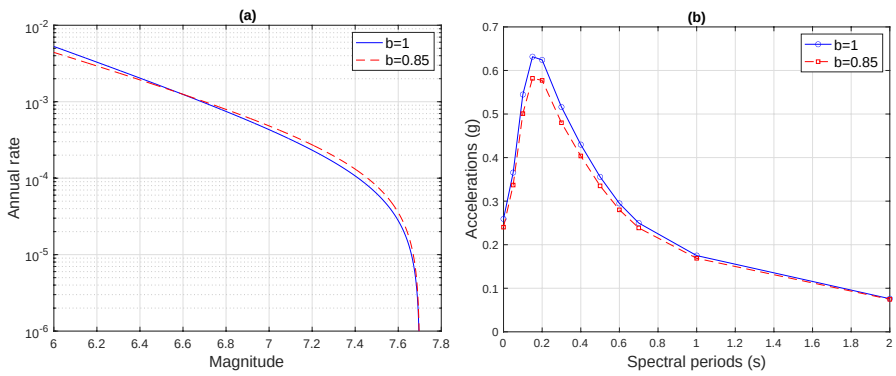

Fig. 12 - (a) Earthquake recurrence model for Mount Lebanon fault, assuming either a b-value of 1.0 or a b-value of 0.85, (b) Associated Uniform hazard Spectrum at Beirut, at 475 yrs return period. Both calculations are led with an M_{max} of 7.7 and mean slip rate.

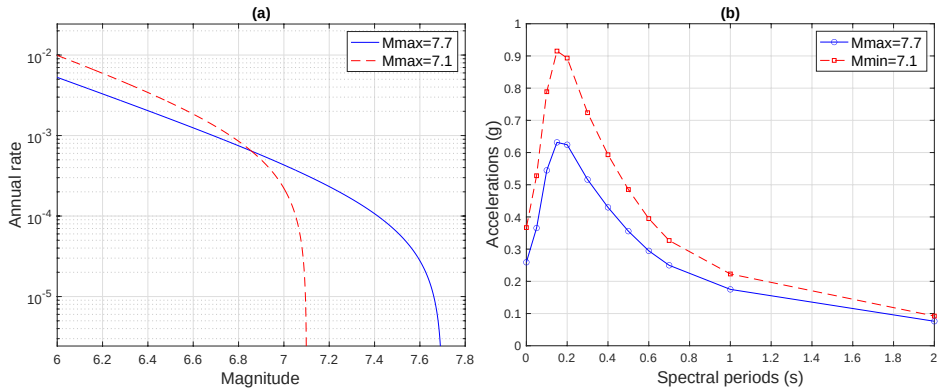

Fig. 13 - (a) Earthquake recurrence model for Mount Lebanon thrust fault, for a given seismic moment (mean slip rate 1.5mm/year), considering alternatively the minimum and the maximum bounds defined for Mmax (Table 2), (b) Uniform hazard spectrum at Beirut, at 475 yrs return period, obtained from the earthquake recurrence models in (a).

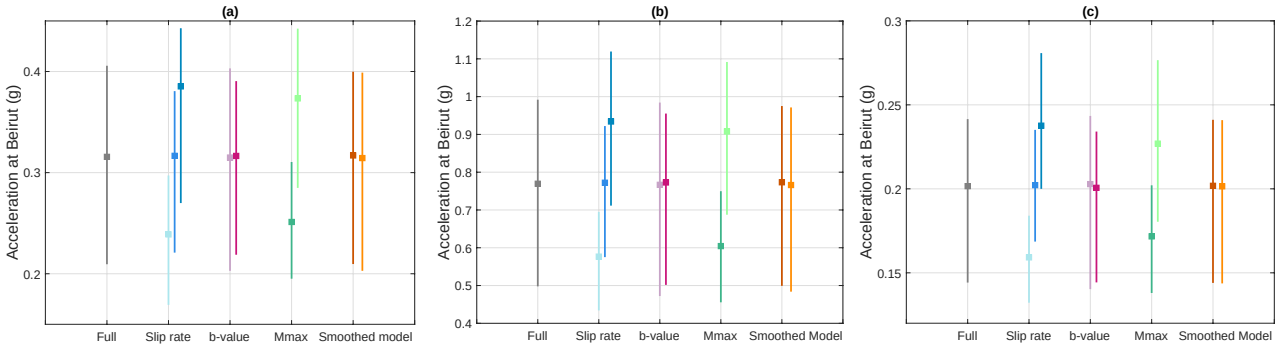

Fig. 14 - Hazard results in Beirut, exploring the source-model logic tree, at 475 years return period. Mean value (square), percentiles 16th and 84th (vertical bar). 'Full': full logic tree, grey (24 branches); 'slip rate': choice of the slip rate (minimum, mean, maximum; light blue to dark blue); 'b-value': choice of the b-value (1.0 or 0.85); choice of the M_{max} (7.7 dark green; 7.1 light green), 'Smoothed Model': choice of the background seismicity model. Spectral period: (a) PGA, (b) 0.2s, (c) 1s.

Table 1 - Fault Parameters

Fault	Mechanism	L(km)	Slip Rate range (mm/yr)	Mean Slip Rate (mm/yr)	Dip (°)	M_{max} from L (Leonard 2010)	Largest historical event associated to the fault	Magnitude of the historial event	M_{max} used
Yammouneh	SS	167	3.8-6.4 (Daeron et al 2007)	5.1	90	7.49 (7.16-7.74)	20 May 1202	Mw=7.6 (Hough and Avni 2009) Ms=7-7.8 (Ambraseys and Jackson 1998)	7.6-7.8 From the historical record
Rachaya	SS	41	1.4±0.2 (Gomez et al 2003)	1.4	90	6.85 (6.56-7.14)	30 Oct 1759	Ms=6.6 (Ambraseys and Barazangi 1989)	6.6-7.1 Scaling relationship using L
Serghaya	SS	90	1.4±0.2 (Gomez et al 2003)	1.4	90	7.22 (6.89-7.47)	25 Nov 1759	Ms=7.4 (7.2-7.5) (Ambraseys and Barazangi 1989)	7.2-7.5 From the historical record
Roum	SS	41	0.86-1.05 (Nemer & Meghraoui 2006)	0.95	90	6.85 (6.56-7.14)	1 Jan 1837	Ms=7.0±0.3 (Ambraseys 2006) Ms=7-7.1 (Ambraseys 1997)	7-7.3 From the historical record
Mount Liban	R	73	1-2 (Elias et al 2007)	1.5	45	7.35 (7.06-7.71)	9 July 551	Ms=7.3 (Darawcheh et al 2000) 7.4-7.6 (Elias et al 2007)	7.1-7.7 Scaling relationship using L
Missyaf	SS	68	4.9-6.3 (Sbeinati et al 2010)	5.6	90	7.03 (6.7-7.28)	29 June 1170	Ms=7±0.3 (Ambraseys 2006)	6.7-7.3 Scaling relationship and historical event
Jordan Gorge Fault	SS	58	$4.1^{+0.4}/_{-1.0}$ (Wechsler et al 2018)	4.1	90	7.1 (6.77-7.35)	18 Jan 746	Ms=7.3±0.3 (Ambraseys 2009) Mw=6.6 (Hough and Avni 2009)	7-7.6 From the historical record

8. References

[1] le Beon, M., Klinger, Y., Amrat, A. Q., Agnon, A., Dorbath, L., Baer, G., Ruegg, J. C., Charade, O., & Mayyas, O. (2008): Slip rate and locking depth from GPS profiles across the southern Dead Sea Transform. Journal of Geophysical Research: Solid Earth, 113(11). https://doi.org/10.1029/2007JB005280

[2] Danciu, L., Şeşetyan, K., Demircioglu, M., Gülen, L., Zare, M., Basili, R., Elias, A., Adamia, S., Tsereteli, N., Yalçın, H., Utkucu, M., Khan, M. A., Sayab, M., Hessami, K., Rovida, A. N., Stucchi, M., Burg, J. P., Karakhanian, A., Babayan, H., … Giardini, D. (2018): The 2014 Earthquake Model of the Middle East: seismogenic sources. Bulletin of Earthquake Engineering, 16(8), 3465–3496. https://doi.org/10.1007/s10518-017-0096-8

[3] Hiemer, S., Woessner, J., Basili, R., Danciu, L., Giardini, D., & Wiemer, S. (2014): A smoothed stochastic earthquake rate model considering seismicity and fault moment release for Europe. Geophysical Journal International, 198(2), 1159–1172. https://doi.org/10.1093/gji/ggu186

[4] Danijel Schorlemmer, Maximilian J. Werner, W. M., Thomas H. Jordan, Yosihiko Ogata, David D. Jackson, Sum Mak, David A. Rhoades, Matthew C. Gerstenberger, Naoshi Hirata, Maria Liukis, Philip J. Maechling, Anne Strader, Matteo Taroni, S. W., , & Jeremy D. Zechar, and J. Z. (2018). Hirata , N ., Liukis , M ., Maechling , P ., Strader , A ., Taroni , M ., Wiemer , S ., Zechar , J . D ., & Zhuang , J . (2018): The Collaboratory for the Study of Earthquake Predictability : Achievements and Priorities . University of Bristol - Explore.

[5] Brax, M., Albini, P., Beauval, C., Jomaa, R., & Sursock, A. (2019): An Earthquake Catalog for the Lebanese Region. Seismological Research Letters, 90(6), 2236–2249. https://doi.org/10.1785/0220180292

[6] Reasenberg, P. (1985): Second-order moment of central California seismicity, 1969–1982. Journal of Geophysical Research: Solid Earth, 90(B7), 5479–5495. https://doi.org/https://doi.org/10.1029/JB090iB07p05479

[7] J. K. Gardner and L.Knopoff. (1974): Is the sequence of earthquakes in southern california, with aftershocks removed, poissonian? The Journal of Geology, 21(3), 288–288. https://doi.org/10.1086/622062

[8] van Stiphout, T., Zhuang, J., & Marsan, D. (2012): Seismicity declustering. Community Online Resource for Statistical Seismicity Analysis, February, 1–25. https://doi.org/10.5078/corssa-52382934.

[9] Gomez, F., Meghraoui, M., Darkal, A. N., Hijazi, F., Mouty, M., Suleiman, Y., Sbeinati, R., Darawcheh, R., Al-Ghazzi, R., & Barazangi, M. (2003): Holocene faulting and earthquake recurrence along the Serghaya branch of the dead sea fault system in Syria and Lebanon. Geophysical Journal International, 153(3), 658–674. https://doi.org/10.1046/j.1365-246X.2003.01933.x

[10] Daëron, M., Klinger, Y., Tapponnier, P., Elias, A., Jacques, E., & Sursock, A. (2007): 12,000-year-long record of 10 to 13 paleoearthquakes on the Yammoûneh fault, levant fault system, Lebanon. Bulletin of the Seismological Society of America, 97(3), 749–771. https://doi.org/10.1785/0120060106

[11] Nemer, T., & Meghraoui, M. (2006): Evidence of coseismic ruptures along the Roum fault (Lebanon): a possible source for the AD 1837 earthquake. Journal of Structural Geology, 28(8), 1483–1495. https://doi.org/10.1016/j.jsg.2006.03.038

[12] Elias, A., Tapponnier, P., Singh, S. C., King, G. C. P., Briais, A., Daëron, M., Carton, H., Sursock, A., Jacques, E., Jomaa, R., & Klinger, Y. (2007): Active thrusting offshore Mount Lebanon: Source of the tsunamigenic A.D. 551 Beirut-Tripoli earthquake. Geology, 35(8), 755–758. https://doi.org/10.1130/G23631A.1

[13] Wechsler, N., Rockwell, T. K., & Klinger, Y. (2018): Variable slip-rate and slip-per-event on a plate boundary fault: The Dead Sea fault in northern Israel. Tectonophysics, 722(October), 210–226. https://doi.org/10.1016/j.tecto.2017.10.017

[14] Sbeinati, M. R., Meghraoui, M., Suleyman, G., Gomez, F., Grootes, P., Nadeau, M. J., Najjar, H. al, & Al-Ghazzi, R. (2010): Timing of earthquake ruptures at the Al Harif Roman aqueduct (Dead Sea fault, Syria) from archaeoseismology and paleoseismology. Special Paper of the Geological Society of America, 471(20), 243–267. https://doi.org/10.1130/2010.2471(20)

[15] Leonard, M. (2010): Earthquake fault scaling: Relating fault length to width , average displacement , and moment release . 47(1), 94.

[16] Anderson, J. G., & Luco, J. E. (1983): Consequences of slip rate constraints on earthquake occurrence relations. Bulletin of the Seismological Society of America, 73(2), 471–496.

[17] Akkar, S., & Çağnan, Z. (2010): A local ground-motion predictive model for Turkey, and its comparison with other regional and global ground-motion models. Bulletin of the Seismological Society of America, 100(6), 2978–2995. https://doi.org/10.1785/0120090367

[18] Akkar et al. (2014): Empirical Ground-Motion Models for Point- and Extended- Source Crustal Earthquake Scenarios in Europe and the Middle East.

[19] Chiou, Brian S. J.Youngs, R. R. (2014): Update of the Chiou and Youngs NGA model for the average horizontal component of peak ground motion and response spectra.

